Role of excited N_2 in the production of nitric oxide

L. Campbell,[1] D. C. Cartwright,[2] and M. J. Brunger[1]

Received 9 February 2007; revised 1 June 2007; accepted 12 June 2007; published 10 August 2007.

[1] Excited N_2 plays a role in a number of atmospheric processes, including auroral and dayglow emissions, chemical reactions, recombination of free electrons, and the production of nitric oxide. Electron impact excitation of N_2 is followed by radiative decay through a series of excited states, contributing to auroral and dayglow emissions. These processes are intertwined with various chemical reactions and collisional quenching involving the excited and ground state vibrational levels. Statistical equilibrium and time step atmospheric models are used to predict N_2 excited state densities and emissions (as a test against previous models and measurements) and to investigate the role of excited nitrogen in the production of nitric oxide. These calculations predict that inclusion of the reaction $N_2[A^3\Sigma_u^+]$ + O, to generate NO, produces an increase by a factor of up to three in the calculated NO density at some altitudes.

Citation: Campbell, L., D. C. Cartwright, and M. J. Brunger (2007), Role of excited N_2 in the production of nitric oxide, *J. Geophys. Res.*, *112*, A08303, doi:10.1029/2007JA012337.

1. Introduction

[2] Radiative decay of the excited states of N_2 has long been identified as the source of many auroral emissions, such as the Vegard-Kaplan (VK) bands from transitions between vibrational levels in $A^3\Sigma_u^+ \rightarrow X^1\Sigma_g^+$. It has been proposed [*Swider*, 1976; *Gordiyets*, 1977] that $N_2[A^3\Sigma_u^+]$ and $N_2[X^1\Sigma_g^+ (\nu' > 11)]$ react with O atoms to produce nitric oxide. These are potentially important chemical processes because although a minor constituent, NO is a vital component of the Earth's atmosphere due to the critical role it plays in determining the thermal balance in the lower thermosphere [*Killeen et al.*, 1997] and in the odd-nitrogen chemistry in the ionosphere [*Strickland et al.*, 1999]. Its density is highly variable [*Adler-Golden et al.*, 1999] and the production mechanisms leading to enhanced NO densities in aurora are complex and not fully understood [*Solomon and Barth*, 1999]. Similarly, NO production by sunlight is a subject of ongoing research [*Barth and Bailey*, 2004], as are the reaction rates involved [*Duff et al.*, 2005].

[3] Motivated by the large variability in the measured and inferred auroral NO densities reported in the early 1970s, *Hyman et al.* [1976] examined the NO chemistry to determine upper limits on the NO concentration and its production rate. They concluded that the NO concentration ([NO]) cannot exceed $0.1 \times [O_2]$ and called attention to the sensitivity of [NO] to the $N(^2D)$ and $N(^4S)$ atoms produced in the odd-nitrogen chemical cycle.

[4] *Swider* [1976] originally proposed the reaction $N_2[A^3\Sigma_u^+]$ + O → NO + $N(^2D)$ as a source of NO, and it was included in a model of NO production by *O'Neil et al.* [1979]. In seeking to explain observations of higher concentrations of NO, *Gordiyets* [1977] showed that the reaction $N_2[X^1\Sigma_g^+ (\nu' > 11)]$ + O → NO + N can also be an important source of NO and *Vlasov et al.* [1980] proposed it as the main source of NO in strong aurora. Its rate is quoted as 10^{-11} cm^3 s^{-1} by *Aladjev and Kirillov* [1995], who ascribe it to Rusanov and Fridman in a publication in Russian. This value is larger than used in some recent work [*Pintassilgo et al.*, 2005].

[5] *Sharma et al.* [2001] have shown that the enhancement of NO infrared emissions observed in the 6.8–10.8 μm band in the 110–130 km region during an auroral event can be explained by the prompt chemiluminescent emission from the nascent NO formed by $N(^2D) + O_2 \rightarrow NO + O$, which is initiated by local auroral energy deposition producing N atoms. In their model the chemical reactions responsible for producing NO in an aurora of characteristic energy 8 keV, were determined to have the relative ranking:

$N(^2D) + O_2 \rightarrow NO + O$	172
$N_2[A^3\Sigma_u^+] + O \rightarrow NO + N(^2D)$	7.4
$N(^2P) + O_2 \rightarrow NO + O$	5
$N(^4S) + O_2 \rightarrow NO + O$	1

Thus Sharma et al. find that the production and loss of $N(^2D)$ is the critical element in the auroral production of NO, but note that the $N_2[A^3\Sigma_u^+]$ reaction is included.

[6] In the current work we utilize a recently developed model that combines the radiative cascade processes in excited nitrogen with a simple photochemical description of atmospheric species [*Campbell et al.*, 2006]. This model has been shown to predict intensities of the Lyman-Birge-Hopfield (transitions between vibrational levels in $a^1\Pi_g \rightarrow$

[1] ARC Centre for Antimatter-Matter Studies, School of Chemistry, Physics and Earth Sciences, Flinders University, Adelaide, South Australia, Australia.
[2] Rush City, Minnesota, USA.

0148-0227/07/2007JA012337

$X^1\Sigma_g^+$) and VK bands [*Campbell et al.*, 2005] in reasonable agreement with rocket and satellite measurements. Comparisons with measurements and other calculations are made here, to verify our model for its estimates of $N_2[A^3\Sigma_u^+]$ densities. The predictions of NO density from our model are compared with those from other models and with measurements to show that our model is sufficiently accurate to be used to investigate the role of $N_2[A^3\Sigma_u^+]$ and $N_2[X^1\Sigma_g^+ (\nu' > 11)]$ in the production of NO. We find that in both equatorial daytime and high-latitude auroral conditions, $N_2[A^3\Sigma_u^+]$ makes a significant contribution to the NO density, while the contribution from $N_2[X^1\Sigma_g^+ (\nu' > 11)]$ is relatively small. As the inclusion of the $N_2[A^3\Sigma_u^+]$ + O reaction will reduce the calculated 557.7 nm emission in aurora, we confirm that our predicted 557.7 nm emission is consistent with auroral measurements. The effect of atmospheric winds on the calculated altitude profile of NO density is also investigated.

2. Details of the Model

[7] The computational model has been extended to altitudes below 120 km using:

$$F_h = F_{120}\ e^{-0.1(120-h)} \quad (1)$$

where F_h is the calculated auroral flux at height h and F_{120} is the flux at 120 km [*Campbell et al.*, 2006]. Equation (1) was chosen to match our predictions of $O(^1S)$ excitation to those of *Sharp et al.* [1979]. Below 100 km the auroral flux is reduced linearly to zero at 89 km, similar to the lower height limit in Figure 4.28 of *Vallance Jones* [1974].

[8] Molecular and eddy diffusion of $N(^4S)$ and NO have been incorporated: Coefficients of molecular diffusion between pairs of constituents [*Pavlov*, 1981] are combined [*Pavlov*, 1988] to give molecular diffusion coefficients. For the equatorial case, measured eddy diffusion coefficients [*Sasi and Vijayan*, 2001] for September are used for the altitude range 70–90 km. Above 100 km the often-used value of 1×10^6 cm^2 s^{-1} [e.g., *Barth*, 1992] is applied, with linear interpolation between this value and that of Sasi and Vijayan at 90 km used for the range 90–100 km. For the auroral case, eddy diffusion coefficients for 20 September are read from a graph of calculated results at 61°N [*Garcia and Solomon*, 1985]. The eddy and molecular diffusion coefficients are used to calculate diffusion rates using equation (E-10) of *Bailey et al.* [2002].

[9] Updated rates for the reactions $N(^2D) + O_2 \rightarrow NO + O$ [*Duff et al.*, 2005], $N(^4S) + O_2 \rightarrow NO + O$ and $N(^4S) + NO \rightarrow N_2 + O$ [*Pintassilgo et al.*, 2005] are used. Otherwise the photochemical model is as described previously [*Campbell et al.*, 2006].

[10] A statistical equilibrium calculation is employed to determine the populations of the excited states of N_2, which are then "imported" into a time step simulation [*Campbell et al.*, 2006] that is used to calculate the NO density. In the latter the incremental change in density $\Delta[z]$ for each species z is calculated at successive time steps of Δt as $\Delta[z] = R[x][y]\Delta t$, where R is the rate for the reaction $x + y \rightarrow z$. Calculations are made at either 0.5 s intervals in the auroral case or 1.0 s in the equatorial case. These intervals are too long for some fast reactions, for which an equilibrium calculation is performed at each time step.

3. Results and Discussion

[11] The current model is verified by comparison of its predictions of $N_2[A^3\Sigma_u^+]$ densities, $N_2[X^1\Sigma_g^+]$ production, $A^3\Sigma_u^+ \rightarrow X^1\Sigma_g^+$ emissions and NO production rates with other models and measurements. It is used to calculate NO densities in conditions for which measurements are available. The calculation is made with and without the NO production due to $N_2[A^3\Sigma_u^+]$ and $N_2[X^1\Sigma_g^+]$ to assess its importance, including the implications for calculations of 557.7 nm emission. The effect of vertical winds in these calculations is assessed by a sample calculation.

3.1. $N_2[A^3\Sigma_u^+]$ in Daytime and Aurora

[12] Figure 1 shows the predicted number density of $N_2[A^3\Sigma_u^+]$ produced by an IBC II^+ aurora and by sunlight for a solar zenith angle of 0°. It shows that the densities due to the aurora are greater than those due to sunlight, ranging from a factor of 15 at 130 km down to about 2 at 200 km and above. The predicted densities for aurora at 130 km without quenching are shown, to allow comparison with the predictions (scaled to the current $N_2[A^3\Sigma_u^+, \nu' = 0]$ density) of *Cartwright* [1978] and *Morrill and Benesch* [1996]. The shape of the distribution differs from that of Cartwright due to the use of updated transition probabilities [*Gilmore et al.*, 1992]. It is similar to that of Morrill and Benesch, who used the transition probabilities of Gilmore et al. However, the densities are about half of those calculated by Cartwright, with only about 10% of this discrepancy being due to the changes in the auroral spectrum and updated cross sections. The densities of Morrill and Benesch are also larger than the current values, but this is not an independent determination because they used excitation rates from *Cartwright* [1978].

[13] Relative distributions deduced in fitting synthetic spectra to observations of dayglow at 200 km [*Broadfoot et al.*, 1997], auroral column emission [*Degen*, 1982], and aurora at 110 km [*Eastes and Sharp*, 1987] are also included in Figure 1 by scaling to the appropriate $N_2[A^3\Sigma_u^+, (\nu' = 0)]$ value. There is good agreement in the shapes of the distributions for aurora, except that the current model does not predict the enhancement for $\nu' = 6$ and $\nu' = 7$ found by Degen. However, this enhancement is not seen in the measurements of *Eastes and Sharp* [1987] and also Degen states that for the vibrational populations, "The values adopted ... are still uncertain and somewhat arbitrary." Hence that enhancement may not be real. For dayglow the measured values [*Broadfoot et al.*, 1997] of the relative populations for levels 0, 1, and 2 agree with the present model. Broadfoot et al. also give theoretical predictions for levels 3–6 which are lower than the current predictions for levels 4–6. These discrepancies however are not accounted for by the processes ($C^3\Pi_u$ predissociation and resonance scattering) that are not in the current model but are included by Broadfoot et al. (The theoretical distributions calculated by Broadfoot et al. with these processes included are closer to our predictions than to their inferred measurements.)

[14] Given the discrepancies in both the absolute and relative values of the calculated $A^3\Sigma_u^+$ populations with previous cases, the current model is tested indirectly by

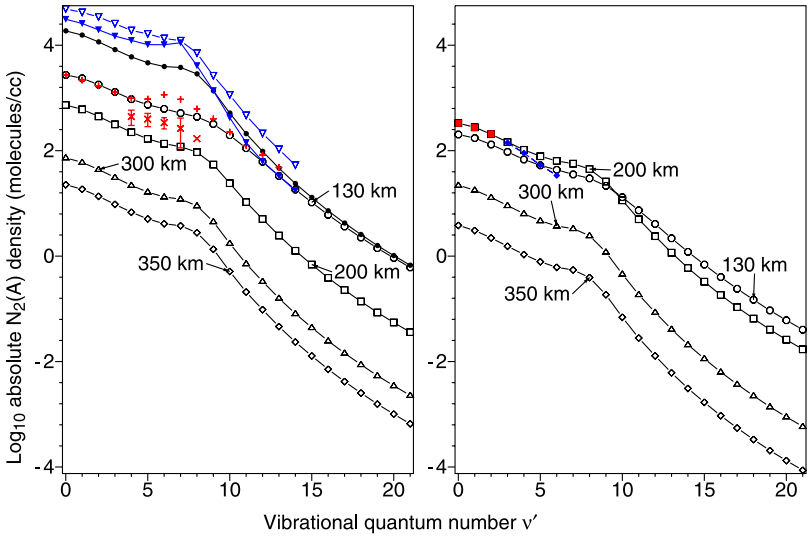

Figure 1. Absolute densities of $N_2[A^3\Sigma_u^+]$ are shown as a function of vibrational quantum number for 130 km (black line of open circles), 200 km (black line of open squares), 300 km (black line of open trianges) and 350 km (black line of open diamonds), for aurora on the left and daytime on the right. Predictions for the densities without quenching, for aurora at 130 km, are shown for the current calculation (black line of solid circles) and for the previous calculations (scaled to the N_2 density of the current model) of *Cartwright* [1978] (blue line of filled triangles) and *Morrill and Benesch* [1996] (blue line of open triangles). Relative values fitted to auroral observations, scaled to the density in the current model of $A^3\Sigma_u^+$ ($\nu' = 0$) at 130 km, are shown for column emission [*Degen*, 1982] (red pluses) and for 110 km [*Eastes and Sharp*, 1987] (red crosses). Relative values for daytime at 200 km [*Broadfoot et al.*, 1997], scaled to $A^3\Sigma_u^+$ ($\nu' = 0$) at 200 km, are shown for measurements (red squares) and calculations (blue line of filled diamonds).

comparison of its predictions of other quantities with previous models and measurements. In Figure 2 calculated values for the production rate of "vibrational quanta" (the sum of the number of transitions to vibrational level ν'' of the ground state, multiplied by ν''), by direct electron impact and $A^3\Sigma_u^+ \rightarrow X^1\Sigma_g^+$ transitions, are compared with the results of *Richards and Torr* [1986]. The present calculation gives production rates of vibrational quanta by direct electron impact that are up to a factor of two different to the those of Richards and Torr, being higher at lower altitudes and lower at higher altitudes. This is not unreasonable as the current model uses an updated set of electron impact cross sections [*Campbell et al.*, 2004] for the vibrational levels. However, while the $A^3\Sigma_u^+$ contribution matches reasonably at higher altitudes, it is significantly lower at the lower altitudes. This is due to different assumptions about collisional quenching. Whereas we assume this returns excited N_2 to the ground state, Richards and Torr presumably use the assumption of *Richards et al.* [1986] that both radiation and atomic oxygen quenching leave N_2 in the same distribution of vibrational levels in the ground electronic state. When the current model is run without quenching, equivalent to the assumption of Richards and Torr that all deactivations of $A^3\Sigma_u^+$ end up in the same distribution of vibrational quanta, our production rates are in much closer agreement with theirs but larger by up to 50%. This difference is not unreasonable given that we have calculated the $A^3\Sigma_u^+ \rightarrow X^1\Sigma_g^+$ transitions in detail, whereas Richards and Torr presumably use the approximation [*Richards et al.*, 1986] that all $A^3\Sigma_u^+ \rightarrow X^1\Sigma_g^+$ tran-

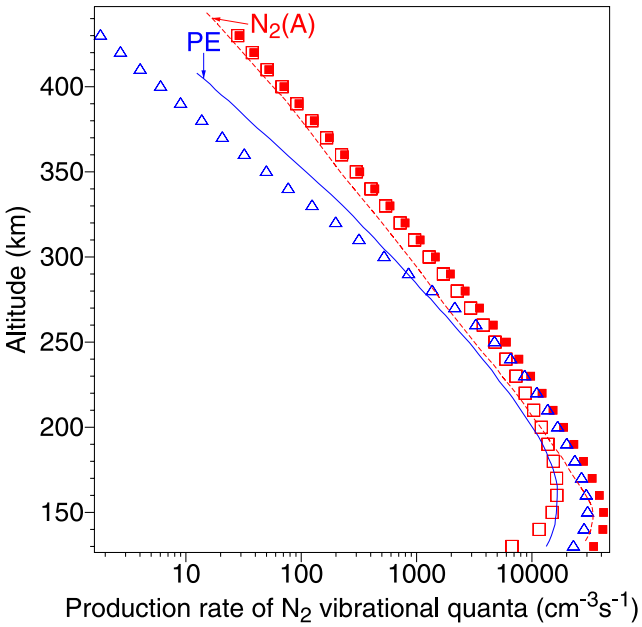

Figure 2. Production rates of N_2 vibrational quanta in daytime. Previous calculations [*Richards and Torr*, 1986] are shown for photoelectron impact (blue solid line) and $A^3\Sigma_u^+ \rightarrow X^1\Sigma_g^+$ transitions (red dotted line). The current calculations are given for photoelectron impact (blue open triangles), $A^3\Sigma_u^+ \rightarrow X^1\Sigma_g^+$ with quenching (red open squares) and $A^3\Sigma_u^+ \rightarrow X^1\Sigma_g^+$ without quenching (red filled squares).

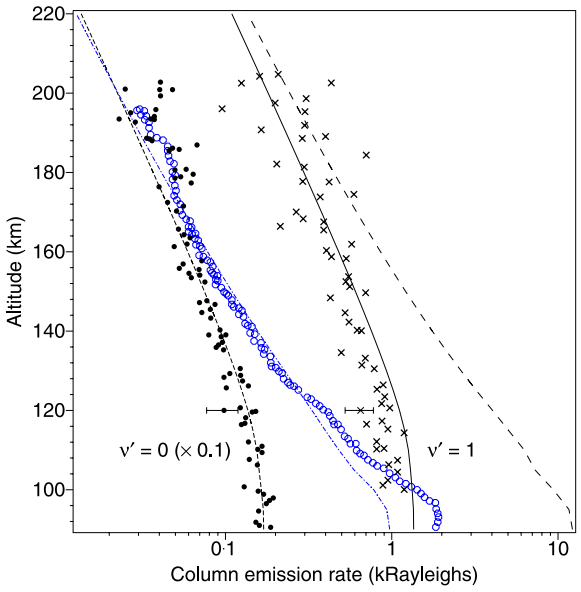

Figure 3. Adjusted measurements [*Sharp*, 1971] of the column emission rate for the downleg portion of a rocket flight into an IBC I^+ aurora, for the sums of all $A^3\Sigma_u^+$ ($\nu' = 0$) → $X^1\Sigma_g^+$ (black filled circles) and of all $A^3\Sigma_u^+$ ($\nu' = 1$) → $X^1\Sigma_g^+$ emissions (black crosses), and the first negative (blue open circles). Predictions of the current model for the first negative (blue dash-dotted line), for $\nu' = 0$ (black short dashed line), and for $\nu' = 1$ with (black solid line) and without (black long dashed line) quenching and chemical reactions. Error bars at 120 km indicate the uncertainty on two example points that show the sum for only the subset of the transitions that were measured. All values for $\nu' = 0$ are multiplied by 0.1 to avoid overlap on the plot.

sitions terminate in $X^1\Sigma_g^+$ ($\nu'' = 7$). The main point is that despite the current $A^3\Sigma_u^+$ populations being less than previously calculated [*Cartwright*, 1978], the unquenched populations are larger than calculated in another model, so there is not a consistent trend that they are underestimated.

[15] In the absence of direct measurements for the densities of the $A^3\Sigma_u^+$ state, the current model can be indirectly validated by comparison with measurements of $A^3\Sigma_u^+$ (ν') → $X^1\Sigma_g^+$ (ν'') emissions. In Figure 3 such measurements are shown for the downleg of a rocket flight into an IBC I^+ aurora [*Sharp*, 1971]. These measurements have a calculated component, in that emissions for only some transitions were measured and the total emission for initial level ν' was calculated by Sharp using the transition probabilities of *Shemansky* [1969] and the measured transitions. Examples of the actual measured values (e.g., the sum of $\nu'' = 5,6,7,8$ for $\nu' = 0$) at 120 km are given by Sharp and shown as the two points with error bars in Figure 3, while the points without error bars show the adjusted measurements of Sharp, i.e., measurements adjusted to include all transitions for $\nu' = 0$ and $\nu' = 1$.

[16] To scale the auroral flux independently of the $A^3\Sigma_u^+$ densities, it was set to give a good match of our predictions of the 427.8 nm first negative ($N_2^+[B^2\Sigma_u^+(0) \rightarrow X^2\Sigma_g^+(1)]$) to those measured by Sharp above 115 km. Our predictions of Sharp's adjusted measurements are shown by the curves in Figure 3. There is good agreement of our predictions of the rates of $A^3\Sigma_u^+(0) \rightarrow X^1\Sigma_g^+(\nu'')$ with the adjusted measurements of Sharp, with an underestimation for $\nu' = 1$. The discrepancies are of the same order as the errors in the measured values, while the errors in the adjusted measurements might be larger due to errors in the transition probabilities used by Sharp in calculating them. Hence the agreement of the current predictions with the measurements is good in view of the experimental variation.

[17] As quenching and chemical reactions cause depletion of excited nitrogen without producing emission, the model was run with these omitted. This results in predicted emissions that are much higher than the measurements at low altitudes. Hence reasonable agreement with the measurements is seen only when the chemical reactions and quenching are included.

[18] While the current model is in disagreement with some previous results, principally in that it gives lower values for the $A^3\Sigma_u^+$ densities than earlier auroral calculations [*Cartwright*, 1978; *Morrill and Benesch*, 1996], it is in reasonable agreement with other calculations [*Richards and Torr*, 1986] for the production of vibrational quanta from $A^3\Sigma_u^+$ in daytime and in good agreement with measurements [*Sharp*, 1971] of auroral emissions produced by radiative decay of the $A^3\Sigma_u^+$ state. This suggests that our predicted densities of the $A^3\Sigma_u^+$ levels are accurate enough for an investigation of the production of NO via the $A^3\Sigma_u^+$ state.

[19] A problem is that in comparing with the available measurements only one parameter is generally available. A useful set of measurements would be simultaneous values of the $N_2[A^3\Sigma_u^+]$ vibrational distribution, the 557.7 nm emission and the NO (2 → 1) infrared emission.

3.2. $N_2[A^3\Sigma_u^+]$ and $N_2[X^1\Sigma_g^+(\nu' > 11)]$ Production of NO

[20] As an initial test the current model is run for similar conditions to those for the model of *Barth* [1992]. In Figure 4 the production rates of NO by various species in the current model are compared with those of Barth. The current model provides a reasonable emulation of that of Barth and so is adequate to investigate the importance of excited N_2. Also included in Figure 4 are the rates of NO production due to the reactions of $N_2[A^3\Sigma_u^+]$ and $N_2[X^1\Sigma_g^+(\nu' > 11)]$ with O, as predicted by our model. These reactions appear unimportant compared to the reactions of N atoms with O_2. However, including them actually increases the calculated NO density by a factor of about 2–3 at lower altitudes, as will be shown below.

[21] To investigate the role of $N_2[A^3\Sigma_u^+]$ and $N_2[X^1\Sigma_g^+(\nu'' > 11)]$ in the production of NO, the model is run with and without the reactions:

$$N_2\left[A^3\Sigma_u^+\right] + O \rightarrow NO + N\left(^2D\right)$$

and

$$N_2\left[X^1\Sigma_g^+(\nu'' > 11)\right] + O \rightarrow NO + N\left(^4S\right),$$

to compare with measurements by the SNOE satellite [*Barth et al.*, 2003] of the NO density.

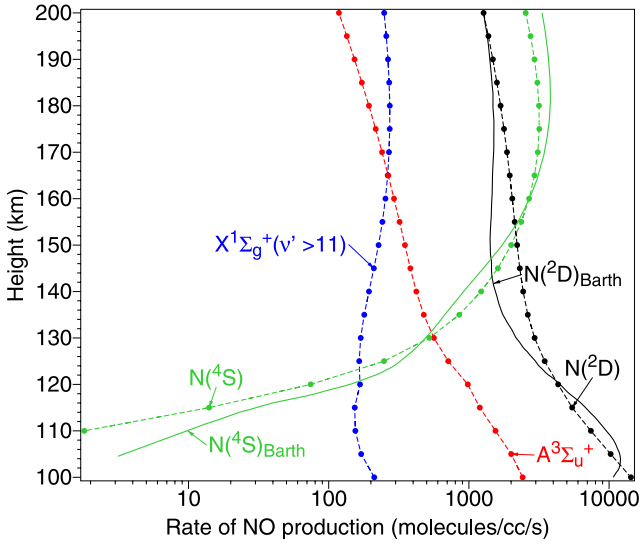

Figure 4. Comparison of current calculations (dashed line of filled circles) with results of *Barth* [1992] (solid lines) for production rates of NO due to reactions involving species as labeled.

[22] In Figure 5 predicted values of NO density are compared with measurements for moderate and high solar activity at the equator at about 1100 LT, averaged over several intervals around the spring and autumn equinoxes. The time step calculations are run for 107 hours from 0600, using the atmospheric densities, temperatures and the $F_{10.7}$ index of 208.8 from the MSISE-90 model (http://modelweb.gsfc.nasa.gov/models/msis.html) for 20 September 2000, a day representative of those with high solar activity that is within one of the observation intervals. It can be seen that the predicted NO densities are tending to values in good agreement with the measurements for high solar activity at 110 km and 150 km but up to ~30% lower at altitudes in between. This is not as good as the agreement obtained by *Barth and Bailey* [2004], but the 30% discrepancy is almost within the sum of the uncertainties that they quote (18% for the measurements and 10% for solar input in the calculation, as shown by error bars on the plot) and within the range of discrepancies between their model and the measurements on other days. The agreement with the measurements is substantially better than given by the empirical model of *Mitra* [1968]. Thus while the model is by no means perfect, its ability to produce reasonable NO densities and a satisfactory shape for the profile with height enables us to use it to investigate the role of excited N_2 in the production of NO.

[23] The comparison of the time step predictions at 1100 LT on the fifth day of calculations with the measurements is replotted in Figure 6, along with the result of calculations which exclude one or both of the reactions of $N_2[X^1\Sigma_g^+ (\nu' > 11)]$ and $N_2[A^3\Sigma_u^+]$ with O. The predicted NO densities are significantly less when both reactions are excluded and are outside the range of uncertainty, particularly in the region of the peak density at about 107 km where they are less by a factor of 1.7. As the reductions are not significantly less when only the $N_2[A^3\Sigma_u^+]$ + O reaction is excluded, it is deduced that the $N_2[X^1\Sigma_g^+ (\nu' > 11)]$ + O reaction is only a minor contributor to the NO density, except above 150 km where its contribution is similar to that of $N_2[A^3\Sigma_u^+]$ + O.

[24] Replacing the updated rate [*Duff et al.*, 2005] for $N(^2D)$ + O_2 with the earlier rate [*Herron*, 1999] (in the case where the excited N_2 is excluded) reduces the NO density above 130 km by amounts similar to omitting the excited N_2 reactions. Below 130 km the effect of the excited N_2 reactions is greater, particularly at the height of the peak density and below, where it is 2–4 times as large.

[25] The enhancement due to the inclusion of excited N_2 seems out of proportion to the relative rates of production in Figure 4, where the contributions from $N_2[A^3\Sigma_u^+]$ and $N_2[X^1\Sigma_g^+ (\nu' > 11)]$ are an order of magnitude less than the maximum for the nitrogen atom rates. This disproportionate effect may be explained by the fact that nitrogen atoms react with NO to destroy it as well as produce it. In contrast, for $N_2[A^3\Sigma_u^+]$ and NO the production mechanism is dominant because the reverse reactions [*Herron*, 1999]:

$$N_2\left[A^3\Sigma_u^+\right] + NO \rightarrow N_2 + NO\left[A^2\Sigma^+\right]$$

and

$$N_2\left[A^3\Sigma_u^+\right] + NO \rightarrow N_2 + N + O$$

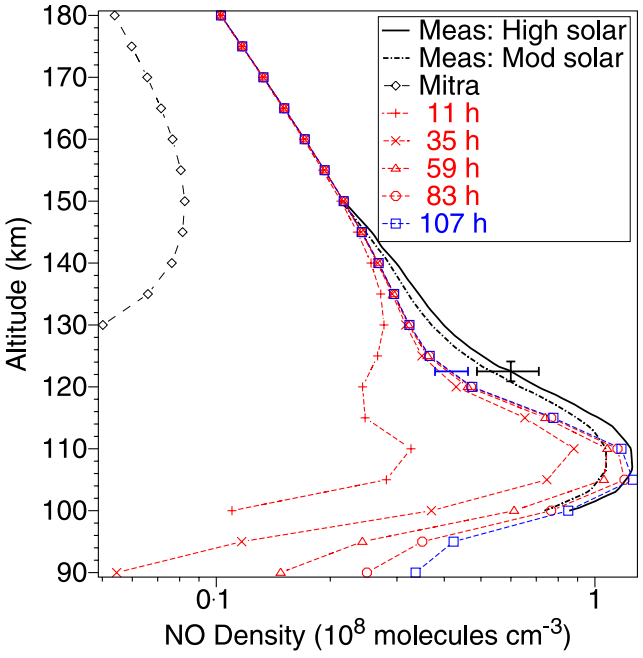

Figure 5. A comparison of the calculated NO density at 1100 LT on successive days of the simulation with the SNOE measurements for high (black solid line) and moderate (black dash-dotted line) solar activitiy and with an empirical model (dashed line of open diamonds) [*Mitra*, 1968]. Error bars at 122.5 km show the estimated measurement uncertainty and the altitude range for the high solar activity case. The error bar shows the estimated uncertainty due to solar input at 122.5 km to the calculated curve for 107 hours.

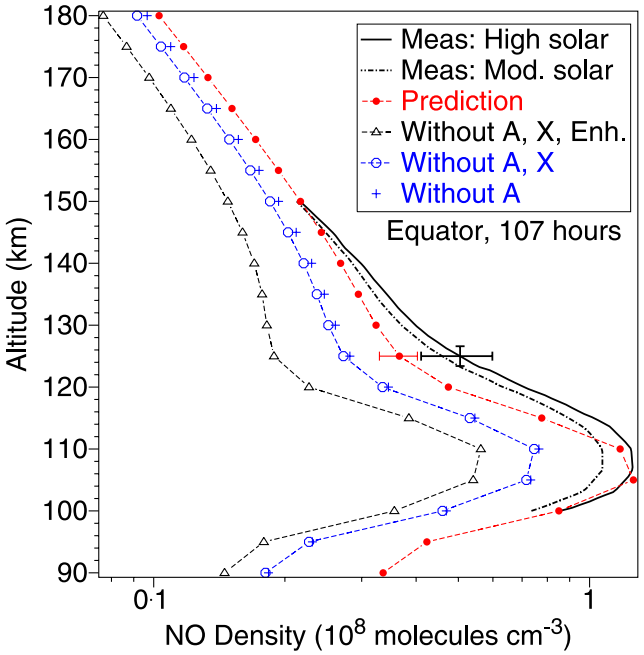

Figure 6. A comparison of the calculated NO densities at 11am after a 4.5-day simulation with the SNOE measurements at the equator for high (black solid line) and moderate (black dash-dotted line) solar activity. The errors bars at 125 km show the estimated measurement uncertainty and altitude range for the high solar activity case. Current calculations including NO production (red line with filled circles) are repeated with successive elimination of the $N_2[A^3\Sigma_u^+]$ (blue pluses) and $N_2[X^1\Sigma_g^+]$ (blue line with open circles) contributions and then replacement of the enhanced rate [*Duff et al.*, 2005] for $N(^2D) + O_2$ by that of *Herron* [1999] (black line with open triangles). The error bar shows the estimated uncertainty due to solar input at 125 km.

only become significant at NO densities much higher than calculated here. A second factor that makes the $N_2[A^3\Sigma_u^+]$ metastable state important in producing NO is that the excited $N(^2D)$ atoms produced by $N_2[A^3\Sigma_u^+] + O$ then take part in other reactions to produce NO, thus further enhancing the contribution by $N_2[A^3\Sigma_u^+]$. This was confirmed by rerunning the model with the $N(^2D)$ product replaced by $N(^4S)$, which at altitudes below 120 km reduced the increase in the NO density by 77–95%.

[26] The analysis is repeated in Figure 7 for the auroral region, now comparing with a previous calculation [*Barth*, 1992] and the SNOE measurements for high geomagnetic activity between 60° and 70° geomagnetic latitude. The calculations are performed for 20 September 2000 at latitude 65°N, longitude 147°W, which is the close to the location for the model of *Barth* [1992] and in the center of the range 60°–70° geomagnetic latitude of the SNOE observations. The calculation is run for only 3.5 days, to give time for the photoelectron component to reach a consistent daily value (as deduced from Figure 5) but to keep the duration of high auroral activity to a reasonably short interval. For a continuous auroral energy flux of 0.5 erg cm^{-2} s^{-1} the calculated profile of NO density is similar to the measurements, but the peak occurs about 5 km lower. This could be due to the characteristic energy (3.1 keV) of our chosen auroral model being high. The lower calculated densities at higher altitudes may be due to the lower height of the peak density because there will be more diffusion downward if the peak density occurs at a lower altitude.

[27] The effect of omitting the $N_2[A^3\Sigma_u^+]$ and $N_2[X^1\Sigma_g^+(\nu' > 11)] + O$ reactions is larger than in the equatorial case, with a 2–3 reduction factor at peak densities. The current model is also run for an auroral energy flux of 1 erg cm^{-2} s^{-1}, which is the value used in the model by *Barth* [1992]. This gives a peak density that is similar to the maximum seen in the SNOE observations and about 4 times that predicted by Barth. This indicates the $N_2[A^3\Sigma_u^+] + O$ reaction has a significant effect and also shows that the current model predicts the maximum measured densities of NO using "standard" levels of auroral activity.

[28] The calculation of *Barth* [1992] was emulated by running the current model, without the excited N_2 reactions and the other updated reaction rates, to match Barth's

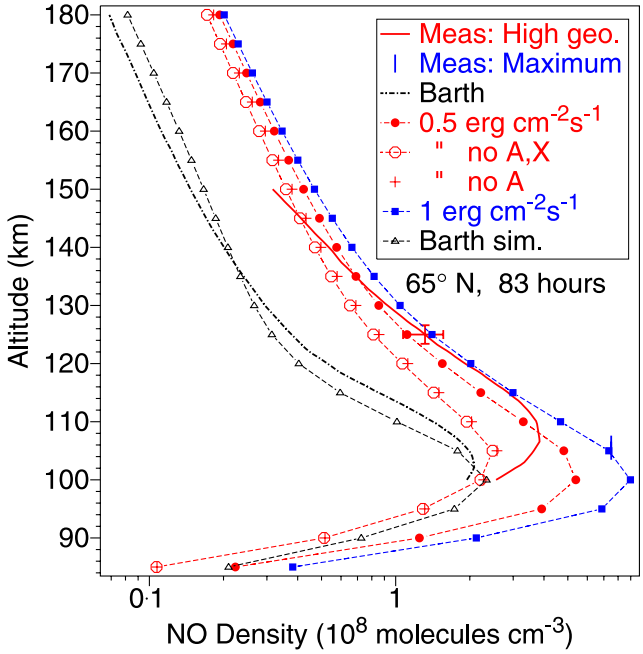

Figure 7. A comparison of calculated NO densities with calculations (black dash-dotted line) [*Barth*, 1992] and with measurements by the SNOE satellite of average densities at 65°N for high geomagnetic activity (red solid line) and the maximum seen (blue vertical line). The current calculations are for high solar activity with auroral activities of 0.5 erg cm^{-2} s^{-1} (red line with solid circles) and 1.0 erg cm^{-2} s^{-1} (blue line with solid squares). The calculations for 0.5 erg cm^{-2} s^{-1} are repeated without the contributions from $N_2[A^3\Sigma_u^+]$ only (pluses) and without the contributions from both $N_2[A^3\Sigma_u^+]$ and $N_2[X^1\Sigma_g^+]$ (red line with open circles). The current calculation, without contributions from $N_2[A^3\Sigma_u^+]$ and $N_2[X^1\Sigma_g^+]$ and without the updated reaction rates, is applied (black line with open triangles) for the conditions of the calculation by Barth.

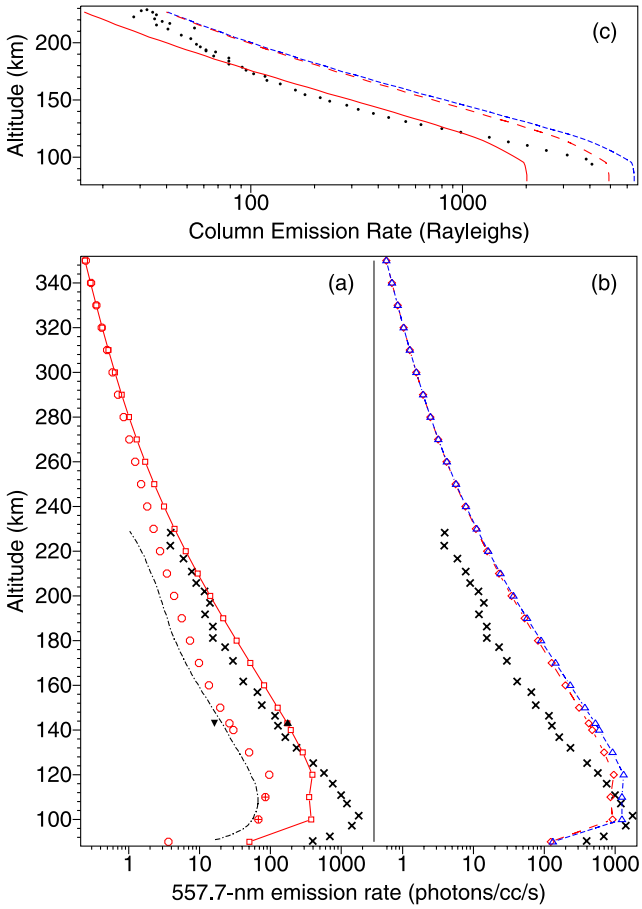

Figure 8. (a) A comparison of the current calculations with previous values [*Sharp et al.*, 1979] of the calculated rate of direct electron impact excitation of O(^{1}S) (dash-dotted line) and measurements of the 557.7 nm emission (black crosses). Rates of O(^{1}S) excitation (black downward pointing filled triangle) and 557.7 nm emission (black upward pointing filled triangle) are calculated using the measured secondary electron spectrum at 143 km. The current calculations of 557.7 nm emission with NO production (red line with open squares) and of direct O(^{1}S) excitation (red open circles) are shown for the implied auroral energy flux of 1.04 erg cm^{-2} s^{-1}. (b) Comparing the measurements with 557.7 nm emission calculated with (red line with open diamonds) and without (blue line with open triangles) NO production, for the specified electron energy flux of 2.54 erg cm^{-2} s^{-1}. (c) Measured values (black dots) [*Sharp et al.*, 1979] of the 557.7 nm column emission rates, and the current calculation of these with (red long-dashed line) and without (blue dashed line) NO production for 2.54 erg cm^{-2} s^{-1}, and for 1.04 erg cm^{-2} s^{-1} with NO production (red solid line).

conditions as closely as possible (i.e., at March equinox with high solar activity of $F_{10.7}$ = 200 and an auroral energy flux of 1 erg cm^{-2} s^{-1}). The similarity to Barth's model supports the validity of the current calculations.

[29] The results of the calculations above suggest the following important conclusions: with models that yield a reasonable estimate of the atmospheric NO density, the reaction of $N_2[A^3\Sigma_u^+]$ with O atoms leads to a significant increase in the calculated NO density, up to a factor of 3 at lower altitudes for high geomagnetic conditions. The inclusion of the reaction of $N_2[X^1\Sigma_g^+ (\nu' > 11)]$ with O leads to a much smaller increase that only becomes apparent at higher altitudes.

3.3. Implication for 557.7 nm Emission

[30] In addition to the production of NO, $N_2[A^3\Sigma_u^+]$ can be deexcited by a reaction with O atoms, producing O(^{1}S), which can then radiatively decay to O(^{1}D), emitting 557.7 nm radiation [*O'Neil et al.*, 1979]. As the reaction of $N_2[A^3\Sigma_u^+]$ to produce NO competes with this process, an important check on our model is that the 557.7 nm emissions are consistent with the assumed atmospheric conditions. In Figure 8a we compare our predictions with measurements by *Sharp et al.* [1979] of 557.7 nm emissions. An auroral flux of 1.04 erg cm^{-2} s^{-1} scaled the electron spectrum in the calculation to direct measurements at 143 km by Sharp et al. This leads to predictions of O(^{1}S) excitation and 557.7 nm emission at 143 km that are close to those of Sharp et al., as shown in Figure 8a. The calculated values of O(^{1}S) excitation and 557.7 nm emission agree well with the values of Sharp et al. at 130–150 km, while overestimating by a factor of up to 2 at higher altitudes and considerably underestimating the 557.7 nm emission at lower altitudes. Note that the agreement for O(^{1}S) excitation below 120 km is expected because the values of Sharp et al. for this quantity were used to determine the height dependence (equation (1)) of the energy flux of our auroral spectrum in the altitude range 100–120 km.

[31] Figure 8b shows the results for repeating the calculation for an auroral flux of 2.54 erg cm^{-2} s^{-1}, which is the value quoted by *Sharp et al.* [1979] for a satellite measurement that was coordinated with the rocket measurement. In this case the predictions are in agreement with the measurements below 120 km.

[32] In Figure 8c the 557.7 nm column emission rates calculated for the two auroral energy fluxes (2.54 and 1.04 erg cm^{-2} s^{-1}) are compared with the values measured by *Sharp et al.* [1979]. The current calculation using the energy flux of 2.54 erg cm^{-2} s^{-1} agrees well at the lowest altitude, while above 120 km there is good agreement using the energy flux of 1.04 erg cm^{-2} s^{-1}.

[33] Thus we are able to predict the correct magnitude of the 557.7 nm emission measured by *Sharp et al.* [1979] at lower altitudes by using the primary electron flux (measured from a satellite) or at higher altitudes by scaling to the secondary electron spectrum measured by a rocket at 143 km. The apparent discrepancy we find in these two cases may be due to auroral variability, coupled with different locations for different observations [*Rees et al.*, 1977]. This may also explain the discrepancy between the shape of the calculated and measured profiles in the height range 100–120 km, as this is the range over which the auroral energy flux seems to change. However, it could also be due, at least in part, to our addition of the new pathway $N_2[A^3\Sigma_u^+] + O \rightarrow NO + N(^2D)$, which would reduce the 557.7 nm emission.

[34] In Figure 8b the result of running the model without the NO production pathway is shown for the energy flux of 2.54 erg cm^{-2} s^{-1}. It indicates that the 557.7 nm emission is

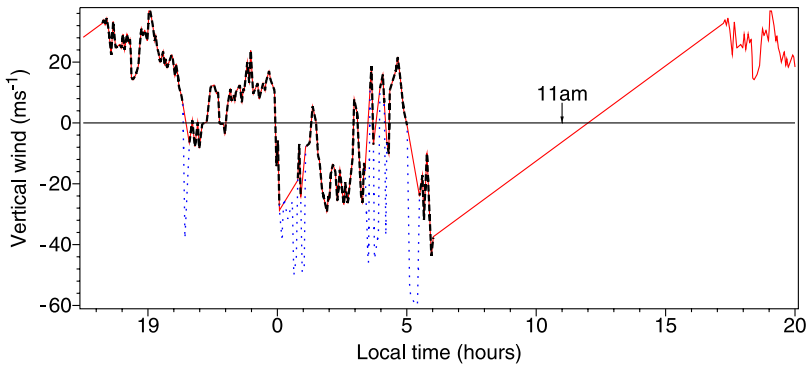

Figure 9. Measurements of vertical neutral wind (positive upward) [*Ishii*, 2005] with low (black dashed line) and high (blue dashed line) error and the fit (red solid line) to these measurements used in this work. The time of the NO measurements (1100 LT) is indicated.

predicted to be up to 30% higher, although there is little difference in the shape of the altitude profile. Thus the effect of including the NO production pathway is smaller than the discrepancies between the model and measurements, although the results when it is included are closer to the measurements for both the definitive values at 143 km and the column emission rate at 100 km.

3.4. Effects of Atmospheric Winds

[35] Significant vertical winds due to auroral heating have been measured [*Price et al.*, 1995], so it is necessary to consider whether the predicted density gradients of NO could exist in the presence of wind. Information on the vertical winds over the time interval and latitude band of the SNOE measurements is not available, so here we calculate the effect of a postulated wind profile based on isolated measurements. Wind is included in the model by calculating, in each time step, the change in density in each height interval due to the amount of NO that is added or removed at the top and bottom of the height interval by the wind.

[36] Measurements of vertical wind, deduced from auroral emissions, at ~120 km over one night [*Ishii*, 2005] are used. It is assumed that the wind pattern is repeated on subsequent nights, and linear interpolation is used over the daylight interval and where the measurement error is large, as shown in Figure 9. The wind speed at 240 km and above is set to 3 times the speed at 120 km, based on the ratios for simultaneous measurements at different heights [*Price et al.*, 1995], with linear interpolation of the speeds between 120 km and 240 km. Below 120 km, assuming conservation of mass, the speed is scaled as the reciprocal of the atmospheric density. These speeds are divided by 20, as we are considering an auroral flux of 0.5 erg cm^{-2} s^{-1}, whereas the measurements are presumed to have been made during an intense aurora. A comparison of the results with these vertical winds with a "no wind" case from Figure 7 is shown in Figure 10. The wind affected case is labeled "downward" as this is the direction prior to the 1100 LT NO measurements. The "upward" case is calculated by running the model with the winds reversed. The postulated vertical winds produce changes of the same order of magnitude as the discrepancies between the calculations and measurements at some altitudes, and also tend to reduce the NO density at 115 km, irrespective of the wind direction. However, the large gradient in NO density remains despite the effect of vertical winds.

[37] It has been suggested that horizontal winds could reduce the NO density by transporting NO out of the auroral zone. *Barth et al.* [2003] postulated a meridional wind of 30 ms^{-1} to account for an observed increase in NO at 106 km at midlatitudes following a large geomagnetic storm. This was questioned by *Richards* [2004], who suggested that it is unlikely that significant transport of NO from high latitudes occurs at this altitude and that other mechanisms could account for the production of the mid-

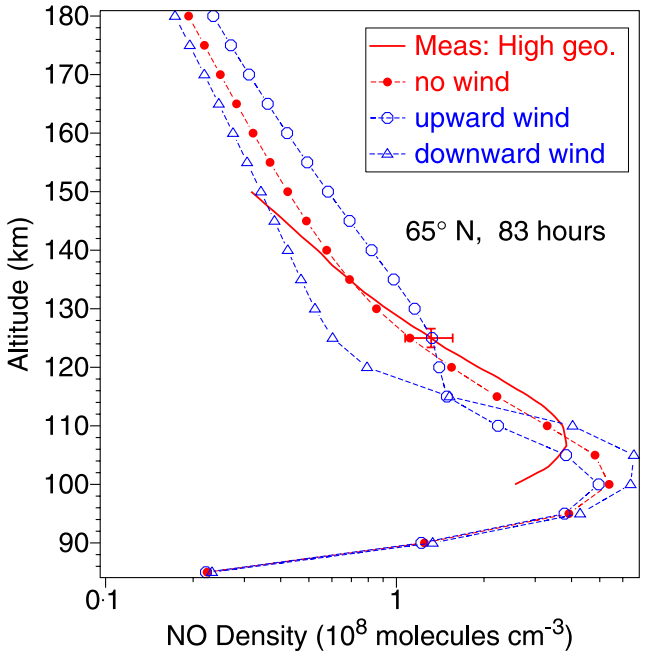

Figure 10. A comparison of calculated NO densities with measurements by the SNOE satellite of average densities at 65°N for high geomagnetic activity (red solid line). The calculations are for high solar activity with auroral activity of 0.5 erg cm^{-2} s^{-1}, without vertical wind (red line with solid circles) and with winds that are upward (blue line with open circles) and downward (blue line with open triangles) before the measurement time.

latitude NO. However, even if this transport occurs, the measurements [*Barth et al.*, 2003, Figure 11] show the postulated transport of NO out of the auroral zone does not occur for most of the time and that when it does the NO density in the auroral region is above average. Thus the one-dimensional calculations here are appropriate for the time-averaged measurements presented by Barth et al. It is expected that horizontal winds would smooth out horizontal variations in NO density created by patchy auroral activity and associated vertical winds. This is consistent with the absence in the measurements of the wind-induced reduction at around 115 km predicted when vertical winds are included in the calculations.

4. Conclusions

[38] An atmospheric model which combines the radiative cascade through the excited states of molecular nitrogen with chemical reactions involving excited nitrogen is used to predict the absolute densities of the vibrational levels of $N_2[A^3\Sigma_u^+]$ and $N_2[X^1\Sigma_g^+]$ and associated emissions. These predictions are compared with various previous simulations and measurements in order to assess the validity of the model, which is then used to investigate the role of vibrationally and electronically excited N_2 in the production of nitric oxide in the atmosphere.

[39] In general, predictions of the $N_2[A^3\Sigma_u^+]$ densities and the associated production of vibrational quanta are consistent with previous simulations, although in some cases discrepancies of a factor of 3 were noted. However, predictions of emissions due to radiative decay of the $N_2[A^3\Sigma_u^+]$ state compare well with measurements in an auroral environment, which supports the overall accuracy of the model employed in this study.

[40] The model was used to predict the NO density in the atmosphere for cases where measurements have been made by satellite: high solar activity at the equator and high geomagnetic activity at high latitudes. At the equator there are discrepancies between the predictions and measurements of $\sim$30% at some altitudes, but there is much better agreement (to $\sim$10%) at the altitude of the peak density. In the auroral case there are discrepancies of up to a factor of two at some altitudes which may be due to the characteristic energy of the auroral model being high. Using two different auroral energy fluxes within a "standard" range, the maximum predicted NO density is shown to be similar to either the average for high geomagnetic activity or to the maximum value observed.

[41] Emulation of a previous calculation showed good agreement for calculated NO densities and suggests that the model employed in this study is sufficient to investigate the role of excited N_2 in the production of NO. This was achieved by running the new model but leaving out either of the production mechanisms involving $N_2[A^3\Sigma_u^+]$ and $N_2[X^1\Sigma_g^+]$. Omitting the $N_2[X^1\Sigma_g^+]$ pathway caused a small reduction above about 150 km and had a negligible effect at lower altitudes. Omitting the $N_2[A^3\Sigma_u^+]$ production mechanism reduced the NO density in the region of the peak by a factor of $\sim$1.7 in the equatorial case and by 2–3 in the auroral case. At altitudes below 130 km the increase in NO density due to excited N_2 is greater than the increase produced by changing to an updated reaction rate for $N(^2D) + O_2$.

[42] Inclusion of the NO production pathway will reduce the predicted 557.7-nm emission, so predictions of the 557.7 nm emission were made, with and without the NO production pathway, and compared with measurements. Inclusion of NO production from $N_2[A^3\Sigma_u^+]$ improved the predictions of 557.7 nm emission, but the improvements were small in comparison to the discrepancies between the calculations and measurements. Inclusion of a vertical wind profile changed the NO density by the same order as the discrepancies between calculations and measurements but did not reduce the large NO density gradients calculated. Thus the effect on the calculated NO density of the $N_2[A^3\Sigma_u^+]$ + O reaction is predicted to be large even in the presence of vertical winds and this conclusion is not invalidated by considering its effect on the 557.7 nm emission.

[43] **Acknowledgments.** This work was supported by the Australian Research Council and Flinders University.

[44] Wolfgang Baumjohann thanks Richard Eastes and another reviewer for their assistance in evaluating this paper.

References

Adler-Golden, S., D. R. Smith, J. Vail, A. Berk, R. Nadile, and L. Jeong (1999), Simulations of mesospheric and thermospheric IR radiance measured in the CIRRIS-1A shuttle experiment, *J. Atmos. Sol. Terr. Phys.*, *61*, 1397–1410.

Aladjev, G. A., and A. S. Kirillov (1995), Vibrational kinetics of molecular nitrogen and its role in the composition of the polar thermosphere, *Adv. Space Res.*, *16*, (l)109–(l)112.

Bailey, S. M., C. A. Barth, and S. C. Solomon (2002), A model of nitric oxide in the lower thermosphere, *J. Geophys. Res.*, *107*(A8), 1205, doi:10.1029/2001JA000258.

Barth, C. A. (1992), Nitric oxide in the lower thermosphere, *Planet. Space Sci.*, *40*, 315–336.

Barth, C. A., and S. M. Bailey (2004), Comparison of a thermospheric photochemical model with Student Nitric Oxide Explorer (SNOE) observations of nitric oxide, *J. Geophys. Res.*, *109*, A03304, doi:10.1029/2003JA010227.

Barth, C. A., K. D. Mankoff, S. M. Bailey, and S. C. Solomon (2003), Global observations of nitric oxide in the thermosphere, *J. Geophys. Res.*, *108*(A1), 1027, doi:10.1029/2002JA009458.

Broadfoot, A. L., D. B. Hatfield, E. R. Anderson, T. C. Stone, B. R. Sandel, J. A. Gardner, E. Murad, D. J. Knecht, and C. P. Pike (1997), N_2 triplet band systems and atomic oxygen in the dayglow, *J. Geophys. Res.*, *102*, 11,567–11,584.

Campbell, L., M. J. Brunger, D. C. Cartwright, and P. J. O. Teubner (2004), Production of vibrationally excited N_2 by electron impact, *Planet. Space Sci.*, *52*, 815–822.

Campbell, L., M. J. Brunger, P. J. O. Teubner, and D. C. Cartwright (2005), Prediction of electron-driven VUV emission in the Earth's atmosphere, *J. Electron Spectrosc. Relat. Phenom.*, *144–147*, 119–122.

Campbell, L., D. C. Cartwright, M. J. Brunger, and P. J. O. Teubner (2006), Role of electronic excited N_2 in vibrational excitation of the N_2 ground state at high latitudes, *J. Geophys. Res.*, *111*, A09317, doi:10.1029/2005JA011292.

Cartwright, D. C. (1978), Vibrational populations of the excited states of N_2 under auroral conditions, *J. Geophys. Res.*, *83*, 517–531.

Degen, V. (1982), Synthetic spectra for auroral studies: the N_2 Vegard-Kaplan band system [1982], *J. Geophys. Res.*, *87*, 10,541–10,547.

Duff, J. W., H. Dothe, and R. D. Sharma (2005), A first-principles model of spectrally resolved 5.3 mm nitric oxide emission from aurorally dosed nighttime high-altitude terrestrial thermosphere, *Geophys. Res. Lett.*, *32*, L17108, doi:10.1029/2005GL023124.

Eastes, R. W., and W. E. Sharp (1987), Rocket-borne spectroscopic measurements in the ultraviolet aurora: the Lyman-Birge-Hopfield bands, *J. Geophys. Res.*, *92*, 10,095–10,100.

Garcia, R. R., and S. Solomon (1985), The effect of breaking gravity waves on the dynamics and chemical composition of the mesophere and lower thermosphere, *J. Geophys. Res.*, *90*, 3850–3868.

Gilmore, F. R., R. R. Laher, and P. J. Espy (1992), Franck-Condon factors, r-centroids, electronic transition moments, and Einstein coefficients for many nitrogen and oxygen band systems, *J. Phys. Chem. Ref. Data*, *21*, 1005–1107.

Gordiyets, V. F. (1977), Vibrational relaxation of anharmonic N_2 molecules and concentration of nitrogen oxide in a disturbed thermosphere, *Geomagn. Aeron.*, *17*, 578–582.

Herron, J. T. (1999), Evaluated chemical kinetics data for reactions of $N(^2D)$, $N(^2P)$, and $N_2(A^3\Sigma_u^+)$ in the gas phase, *J. Phys. Chem. Ref. Data*, *28*, 1453–1483.

Hyman, E., D. J. Strickland, P. S. Julienne, and D. F. Strobel (1976), Auroral NO concentrations, *J. Geophys. Res.*, *81*, 4765–4769.

Ishii, M. (2005), Relationship between thermospheric vertical wind and the location of ionospheric current in the polar region, *Adv. Polar Upper Atmos. Res.*, *19*, 63–70.

Killeen, T. L., A. G. Burns, J. Azeem, S. Cochran, and R. G. Roble (1997), A theoretical analysis of the energy budget in the lower thermosphere, *J. Atmos. Solar Terr. Phys.*, *59*, 675–689.

Mitra, A. P. (1968), A review of D-region processes in non-polar latitudes, *J. Atmos. Terr. Phys.*, *30*, 1055–1114.

Morrill, J. S., and W. M. Benesch (1996), Auroral N_2 emissions and the effect of collisional processes on N_2 triplet state vibrational populations, *J. Geophys. Res.*, *101*, 261–274.

O'Neil, R. R., E. T. P. Lee, and E. R. Huppi (1979), Auroral $O(^1S)$ production and loss processes: Ground-based measurements of the artificial auroral experiment Precede, *J. Geophys. Res.*, *84*, 823–833.

Pavlov, A. V. (1981), Binary molecular diffusion coefficients of neutral components of the upper atmosphere of Earth, Mars and Venus, *Cosmic Res.*, Engl. Transl., *19*, 57–61.

Pavlov, A. V. (1988), The role of vibrationally excited nitrogen in the ionosphere, *Pure Appl. Geophys.*, *127*, 529–544.

Pintassilgo, C. D., J. Loureiro, and V. Guerra (2005), Modelling of a N_2–O_2 flowing afterglow for plasma sterilization, *J. Phys. D Appl. Phys.*, *38*, 417–430, doi:10.1088/0022-3727/38/3/011.

Price, G. D., R. W. Smith, and G. Hernandez (1995), Simultaneous measurements of large vertical winds in the upper and lower thermosphere, *J. Atmos. Terr. Phys.*, *57*, 543–631.

Rees, M. H., A. I. Stewart, W. E. Sharp, P. B. Hays, R. A. Hoffman, L. H. Brace, J. P. Doering, and W. K. Peterson (1977), Coordinated rocket and satellite measurements of an auroral event: 1. Satellite observations and analysis, *J. Geophys. Res.*, *82*, 2250–2258.

Richards, P. G. (2004), On the increases in nitric oxide density at midlatitudes during ionospheric storms, *J. Geophys. Res.*, *109*, A06304, doi:10.1029/2003JA010110.

Richards, P. G., and D. G. Torr (1986), A factor of 2 reduction in theoretical F2 peak electron density due to enhanced vibrational excitation of N_2 in summer at solar maximum, *J. Geophys. Res.*, *91*, 11,331–11,336.

Richards, P. G., D. G. Torr, and W. A. Abdou (1986), Effects of vibrational enhancement of N_2 on the cooling rate of ionospheric thermal electrons, *J. Geophys. Res.*, *91*, 304–310.

Sasi, M. N., and L. Vijayan (2001), Turbulence characteristics in the tropical mesosphere as obtained by MST radar at Gadanki (13.5°N, 79.2°E), *Ann. Geophys.*, *19*, 1019–1025.

Sharma, R. D., R. O'Neil, H. Gardiner, J. Gibson, H. Dothe, J. W. Duff, P. P. Wintersteiner, and M. Kendra (2001), Midcourse Space Experiment: Auroral enhancement of nitric oxide medium-wave infrared emission observed by the Spatial Infrared Imaging Telescope III radiometer, *J. Geophys. Res.*, *106*, 21,351–21,365.

Sharp, W. E. (1971), Rocket-borne spectroscopic measurements in the ultraviolet aurora: Nitrogen Vegard-Kaplan bands, *J. Geophys. Res.*, *76*, 987–1005.

Sharp, W. E., M. H. Rees, and A. I. Stewart (1979), Coordinated rocket and satellite measurements of an auroral event: 2. The rocket observations and analysis, *J. Geophys. Res.*, *84*, 1977–1985.

Shemansky, D. E. (1969), N_2 Vegard–Kaplan system in absorption, *J. Chem. Phys.*, *51*, 689–700.

Solomon, S. C., and C. A. Barth (1999), Auroral production of nitric oxide measured by the SNOE satellite, *Geophys. Res. Lett.*, *26*, 1259–1262.

Strickland, D. J., J. Bishop, J. S. Evans, T. Majeed, P. M. Shen, R. J. Cox, R. Link, and R. E. Huffman (1999), Atmospheric Ultraviolet Radiance Integrated Code (AURIC): Theory, software architecture, inputs, and selected results, *J. Quant. Spectrosc. Radiat. Transfer*, *62*, 689–742.

Swider, W. (1976), Atmospheric formation of NO from $N_2(A^3\Sigma)$, *Geophys. Res. Lett.*, *3*, 335–337.

Vallance Jones, A. (1974), *Aurora*, D. Reidel, Boston, Mass.

Vlasov, M. N., Y. V. Mishin, and V. A. Telegin (1980), Mechanism of formation of high nitric oxide concentrations in the polar ionosphere (English translation), *Geomagn. Aeron.*, *20*, 36–38.

M. J. Brunger and L. Campbell, ARC Centre for Antimatter-Matter Studies, School of Chemistry, Physics and Earth Sciences, Flinders University, GPO Box 2100, Adelaide, SA 5001, Australia. (laurence.campbell@flinders.edu.au)

D. C. Cartwright, 52429 Belle Isle Drive, Rush City, MN 55069, USA.